The Astrophysical Journal Letters, 886:L22 (5pp), 2019 November 20 https://doi.org/10.3847/2041-8213/ab55e2

A Bright Electromagnetic Counterpart to Extreme Mass Ratio Inspirals

Y. Y. Wang[1], F. Y. Wang[1,2], Y. C. Zou[3], and Z. G. Dai[1,2]
[1] School of Astronomy and Space Science, Nanjing University, Nanjing 210093, People's Republic of China; fayinwang@nju.edu.cn
[2] Key Laboratory of Modern Astronomy and Astrophysics (Nanjing University), Ministry of Education, Nanjing 210093, People's Republic of China
[3] School of Physics, Huazhong University of Science and Technology, Wuhan 430074, People's Republic of China
Received 2019 August 22; revised 2019 November 7; accepted 2019 November 9; published 2019 November 20

Abstract

The extreme mass ratio inspiral (EMRI), defined as a stellar-mass compact object inspiraling into a supermassive black hole (SMBH), has been widely argued to be a low-frequency gravitational-wave (GW) source. Providing accurate measurements of the black hole mass and spin of EMRIs is one of the primary interests for the Laser Interferometer Space Antenna (LISA). However, it is currently understood that there are no electromagnetic (EM) counterparts to EMRIs. Here we show a new formation channel of EMRIs with tidal disruption flares as EM counterparts. In this scenario, flares can be produced from the tidal stripping of the helium (He) envelope of a massive star by an SMBH. The remaining compact core of the massive star then evolves into an EMRI. We find that, under a certain initial eccentricity and semimajor axis, the GW frequency of the inspiral can enter the LISA band within $10 \sim 20$ yr, which makes the tidal disruption flare an EM precursor to an EMRI. Although the event rate is just $2 \times 10^{-4}\ \mathrm{Gpc^{-3}\ yr^{-1}}$, this association not only improves the localization accuracy of LISA and helps us to find the host galaxy of EMRI, but it also serves as a new GW standard siren for cosmology.

Unified Astronomy Thesaurus concepts: Gravitational wave sources (677); Tidal disruption (1696); Accretion (14)

1. Introduction

The detection of GW170817/GRB 170817A heralded the era of gravitational-wave (GW) multimessenger astronomy (Abbott et al. 2017a). The neutron star (NS)–NS and NS–black hole (BH) mergers accompanied by electromagnetic (EM) counterparts offer a standard siren for cosmology, which can independently constrain the Hubble constant H_0 (Abbott et al. 2017b; Chen et al. 2018; Wang et al. 2018), calibrate luminosity correlations of γ-ray bursts (Wang & Wang 2019), and so on. In addition to mergers of compact binaries, the extreme mass ratio inspiral (EMRI) (Gair et al. 2013; Amaro-Seoane et al. 2017a; Babak et al. 2017), which originates from the inspiral of a compact object into a supermassive black hole (SMBH), is another source of GWs. Detecting EMRIs is one of the most crucial scientific goals of future space-based GW detectors such as the Laser Interferometer Space Antenna (LISA; Danzmann et al. 2000; Phinney 2002; Amaro-Seoane et al. 2017b; Babak et al. 2017; Amaro-Seoane 2018), the TianQin Project (Luo et al. 2016), and the Taiji Program (Hu & Wu 2017). Nevertheless, LISA can only determine the sky location and luminosity distance of an EMRI to a few square degrees (Cutler 1998) and 10% precision (Babak et al. 2017), respectively, which may not identify the host galaxy uniquely. In this case, statistical methods are required to determine the host galaxy. However, the redshift obtained in this way is not independent of the luminosity distance (Amaro-Seoane et al. 2017a). On the contrary, the EMRIs, if they do have EM counterparts, will serve as a powerful standard siren. However, it seems that there is no EM signal accompanying EMRIs (Amaro-Seoane et al. 2017a), which poses the main obstacle for cosmological application.

The "standard" formation channel of EMRIs is the capture of a compact object (white dwarf (WD), NS, or BH) by an SMBH (Sigurdsson & Rees 1997; Amaro-Seoane et al. 2017a). Other processes include tidal separation of compact binaries, the formation or capture of massive stars in accretion disks, and so on (Amaro-Seoane et al. 2017a; Maggiore 2018).

In this Letter, we utilize a new formation channel for EMRIs. In our model, the EMRI signal comes from the inspiral of a massive star that was tidally stripped by an SMBH. Our Letter is organized as follows. In Section 2, we describe the tidal stripping of massive star's envelopes. The structure and orbital evolution of the remnant core are introduced in Section 3. The signal-to-noise ratio (S/N) of the EMRI is estimated in Section 4. A discussion of the EMRI rate and a brief summary are given in Sections 5 and 6, respectively.

2. Tidal Stripping of Stellar Envelope and Flares

When a star passes close enough through an SMBH, it will be torn apart by the tidal force (Hills 1975; Rees 1988; Evans & Kochanek 1989; Phinney 1989). A star with density ρ is tidally disrupted when the work exerted over it by the tidal force exceeds its binding energy (Rees 1988; Amaro-Seoane 2018). The tidal radius can be calculated from

$$R_{\rm T} \simeq R_*\left(\frac{M_{\rm BH}}{M_*}\right)^{1/3} = \left(\frac{3M_{\rm BH}}{4\pi\rho}\right)^{1/3}, \quad (1)$$

where $M_{\rm BH}$ is the mass of the BH, and R_* and M_* are the stellar radius and stellar mass, respectively. The penetration factor β defines the strength of the tidal interaction exerted on the star (Carter & Luminet 1982)

$$\beta = \frac{R_T}{R_p}, \quad (2)$$

where $R_p = a(1-e)$ is the pericenter.

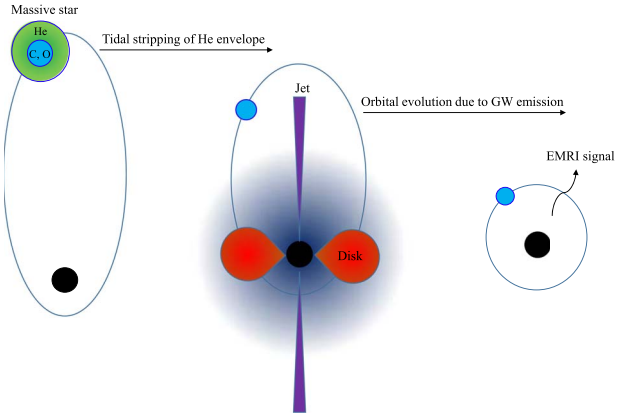

Figure 1. Schematic diagram of the mechanism for observing EMRI and relevant tidal disruption EM signal in our model. Initially, an onion-skin layered massive star orbits an SMBH. After the He envelope gets tidally stripped, X-ray flares are produced by the accretion flow. In some cases, a relativistic jet could be launched by the accreting SMBH. Eventually, the remaining compact C–O core with density about 10^6 g cm^{-3} will inspiral into the SMBH and produce an EMRI signal in the LISA band.

In addition to the whole star, the envelopes of evolving stars can also be tidally stripped. For example, the ultraviolet-optical transient PS1-10jh can be explained by the tidal disruption of a helium-rich stellar core, which is considered the remnant of a tidally stripped red giant (RG) star (Gezari et al. 2012). Furthermore, Bogdanović et al. (2014) studied the tidal stripping of an RG star's envelope by an SMBH and the subsequent inspiral of the core toward the BH. Typically, a massive star has a so-called "onion-skin" structure at the end of its evolution, where each shell has different chemical compositions and mass densities (Woosley et al. 2002). The outer layers have much lower densities than the core, which makes them more vulnerable to tidal forces. Therefore, a massive star may lose its envelopes partially or completely when it passes close enough through an SMBH, leaving a dense core on a highly eccentric orbit (Di Stefano et al. 2001; Kobayashi et al. 2004; Davies & King 2005; Guillochon & Ramirez-Ruiz 2013; Amaro-Seoane et al. 2017a). The tidal disruption flares of main sequence stars and helium stars accompanied by GW bursts have been investigated previously (Kobayashi et al. 2004). However, this type of GW burst cannot be observed if the luminosity distance d_L is larger than 20 Mpc (Kobayashi et al. 2004), which limits its cosmological applications.

Here, we propose a new formation channel for EMRIs with EM precursors. In our model, we assume that a massive star has lost H envelope during the red supergiant period. It is in the He burning stage (Heger et al. 2003) and the densities of different layers vary from 10^{0-3} g cm^{-3} (He envelope) to 10^{5-6} g cm^{-3} (carbon–oxygen (C–O) core; Woosley et al. 2002). After the He envelope is tidally stripped by the SMBH and the C–O core finally inspirals into the SMBH, we can detect a tidal disruption event (TDE) and the subsequent EMRI signal. For a TDE, we can identify the host galaxy and determine the redshift using spectral line observation. With the luminosity distance d_L from the EMRI signal and the redshift z, we have a new type of standard siren. The luminosity distance can be determined to 10% precision at $z = 1$. Figure 1 shows a schematic picture of our model.

Since the typical density of He envelope is 10^3 g cm^{-3} (Woosley et al. 2002) , the tidal stripping should take place in an orbit of semimajor axis $a \sim$ a few 10^{-6} pc and eccentricity $e = 0.90 \sim 0.98$. For our scenario to work successfully, the tidal radius of the He envelope $R_{\rm T,He}$ should be larger than the innermost stable circular orbit (ISCO) radius $R_{\rm ISCO}$. Meanwhile, the tidal radius of C–O core $R_{\rm T,C-O}$ should be smaller than $R_{\rm ISCO}$. Therefore, the feasible mass range of the central SMBH is approximately $3 \times 10^4 \sim 8 \times 10^5 M_\odot$.

Below we show the observational properties of the tidal disruption flare in our model. The energy required to strip the stellar envelope is (Davies & King 2005)

$$E_{\rm strip} \sim \frac{GM_c M_e}{R_c}, \tag{3}$$

where M_c, R_c and M_e are core mass, core radius, and stripped envelope mass, respectively. If the tidal disruption happens on a highly eccentric orbit, about half of the debris will fall back to the BH, in which case the luminosity of the TDE is supposed to follow the standard $t^{-5/3}$ decay rate (Rees 1988; Evans & Kochanek 1989; Phinney 1989). For a 15 $M_\odot$ star, the masses of the core and stellar debris are about 3 $M_\odot$ and 1$M_\odot$, respectively. Assuming that f is the fraction of the accreted stellar envelope relative to the massive star, then the bound material returns to pericenter at a rate

$$\begin{aligned}\dot{M} &\simeq \frac{1}{3}\frac{fM_*}{P_{\rm min}}\left(\frac{t}{P_{\rm min}}\right)^{-5/3} \\ &\simeq 6 \times 10^2 M_\odot\ {\rm yr}^{-1}\left(\frac{f}{0.25}\right) \\ &\cdot \left(\frac{R_*}{10^{10}\ {\rm cm}}\right)^{-3/2}\left(\frac{M_*}{4M_\odot}\right)^2\left(\frac{M_{\rm BH}}{10^5 M_\odot}\right)^{-1/2}\left(\frac{t}{P_{\rm min}}\right)^{-5/3},\end{aligned} \tag{4}$$

where

$$\begin{aligned}P_{\rm min} &= \frac{2\pi R_p^3}{(GM)^{1/2}(2R_*)^{3/2}} \\ &\simeq 6 \times 10^3\ {\rm s}\left(\frac{R_*}{10^{10}\ {\rm cm}}\right)^{3/2}\left(\frac{M_*}{4M_\odot}\right)^{-1} M_5^{1/2},\end{aligned} \tag{5}$$

is the shortest Keplerian orbital period (Ulmer 1999; Bogdanović et al. 2014); M_5 is defined as $M_5 \equiv M_{\rm BH}/(10^5 M_\odot)$.

The luminosity of the accretion flow falling back to the SMBH is (Bogdanović et al. 2014)

$$\begin{aligned}L &= \epsilon \dot{M} c^2 \\ &\simeq 2 \times 10^{48}\ {\rm erg\ s}^{-1}\left(\frac{f}{0.25}\right)\left(\frac{\epsilon}{0.057}\right)\left(\frac{R_*}{10^{10}\ {\rm cm}}\right)^{-3/2} \\ &\cdot \left(\frac{M_*}{4M_\odot}\right)^2 M_5^{-1/2}\left(\frac{t}{P_{\rm min}}\right)^{-5/3},\end{aligned} \tag{6}$$

where $\epsilon = 1 - (r-2)/[r(r-3)]^{1/2}$ is the radiative efficiency for a Schwarzschild black hole and r is the orbital radius of the debris in units of R_g (Bogdanović et al. 2014). The luminosity can be significantly larger than the Eddington limit for a period of weeks to years (Strubbe & Quataert 2009). When $e \leqslant e_{\rm crit} = 1 - 2q^{-1/3}/\beta$, where $\beta \equiv M_{\rm BH}/M_*$, the event is categorized as an eccentric TDE (Hayasaki et al. 2018) and all of the debris will remain gravitationally bound to the SMBH. In these cases, the mass fallback rate is flatter and slightly higher than the standard rate (Hayasaki et al. 2018). Besides, the fallback rate and TDE light curve of more centrally

concentrated stars show a significant deviation from the $t^{-5/3}$ decay rate (Lodato et al. 2009; Dai et al. 2013; Hayasaki et al. 2013; Bogdanović et al. 2014).

The spectra of tidal flares, which are a superposition of blackbody spectrum and many emission lines, are very complicated (Strubbe & Quataert 2009). The temperature of the debris is

$$T_{\rm eff} = \left(\frac{L}{16\pi R_T^2 \sigma}\right)^{1/4} \simeq 2 \times 10^5 \,{\rm K}\, M_5^{1/12}. \quad (7)$$

The luminosity L of the X-ray flares from accretion flow falling back to the SMBH is about 10^{48} erg s^{-1} as estimated above. For the Einstein Probe, which is currently under construction and will have a field of view of 3600 square degrees, the flux sensitivity can be up to 10^{-10} erg cm^{-2} s^{-1} (Yuan et al. 2015). Hence, the Einstein Probe will be able to detect the X-ray flares at $z \geqslant 1.0$. In some cases, a TDE is accompanied by a relativistic jet, which has been observed, for example, in the transient Swift J1644+57 (Bloom et al. 2011; Burrows et al. 2011; Zauderer et al. 2011). If the jet points to us, its luminosity will be much higher than that of the accretion flow.

3. Structure and Orbital Evolution of the Compact Core

3.1. Radius Expansion after Tidal Stripping

After the He envelope is stripped, the core has to adjust to a new equilibrium by expanding its radius. For solar-type stars, the core expansion had been extensively discussed using the mass–radius relation for the adiabatic evolution of a nested polytrope (Hjellming & Webbink 1987; MacLeod et al. 2013; Bogdanović et al. 2014). However, MacLeod et al. (2013) demonstrated that the assumptions for the mass–radius relation are incorrect. Therefore, we perform a rough estimation of the new radius using a hydrostatic equilibrium equation, the first law of thermodynamics, and the relation between the pressure and internal energy density instead. The 15 $M_\odot$ stars model of Woosley & Heger (https://2sn.org/stellarevolution/) is used to estimate the pressure in the outer layer of the C–O core before expansion. According to Pols (2011), the ideal gas assumption is taken for the He envelope and the C–O core. We find that the core's radius will increase by just 16%, which may not affect the tidal radius greatly.

3.2. Requirements for EMRI Formation

In order for a compact object to become an EMRI, its orbital decay timescale by GW emission $\tau_{\rm GW}$ (Gair et al. 2006) should be sufficiently shorter than the two-body relaxation timescale $t_{\rm rlx}$ (Amaro-Seoane et al. 2017a),

$$\tau_{\rm GW} < C_{\rm EMRI}(1-e)t_{\rm rlx}. \quad (8)$$

where $C_{\rm EMRI}$ is a numerical constant sufficiently less than 1, and $t_{\rm rlx}$ is about 10^9 yr. Otherwise, the compact core will be deflected from its original orbit through two-body relaxation.

There is also a limitation on eccentricity e. The maximal eccentricity for a non-plunging orbit is (Cutler et al. 1994; Hopman & Alexander 2005)

$$e_{\rm max}(a) = -\frac{R_{\rm S}}{2a} + \sqrt{\left(\frac{R_{\rm S}}{2a}\right)^2 - \frac{3R_{\rm S}}{a} + 1}\,, \quad (9)$$

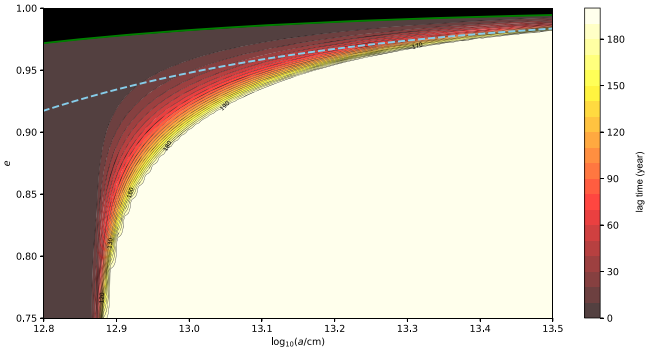

Figure 2. Contour of lag time between TDE and EMRI signal for different initial values of a_0 and e_0. The mass of the SMBH is chosen as $3 \times 10^5 M_\odot$. The blue dashed line refers to the tidal radius R_T, where the He envelope (the density is taken to be 10^3 g cm^{-3}) is disrupted. In the upper-left brown region, the lag times are less than a decade, which are ideal for observing the TDE and EMRI association. The upper-left black region represents the direct plunge orbit, and the green solid line is the upper limit for non-plunging orbit. In the bottom-right region of the diagram, the lag times are all larger than 200 yr and are not shown in detail in the contour.

which is depicted in Figure 2 by the green dashed line.

3.3. Time Lag between the TDE and EMRI Signal

Here, we consider the orbital evolution of the C–O core inspiral. It is reasonable to assume that the He envelope is completely stripped after several close encounters. Hence, the interaction between the diffuse envelope and the core can be neglected here (Amaro-Seoane et al. 2017a). Furthermore, as a is only a few 10^{-6} pc, the encounters of the compact core with cluster stars around the SMBH are ignored.

The semimajor axis a will shrink due to GW radiation. The Keplerian orbital evolution is given by Peters formalism (Peters 1964), which is a good approximation in a weak-field regime. Here there is an important factor that should be taken seriously—the lag time between the tidal disruption and the EMRI signal. The EMRI enters the LISA band when its frequency f, which is twice the Keplerian orbital frequency $f_{\rm orb} = (GM/4\pi a^3)^{1/2}$, is larger than 10^{-4} Hz. It was estimated that, for a binary system consisting of a main-sequence star and a compact object, the latter will spend 10^2–10^4 yr to spiral into the SMBH after the main-sequence star gets tidally disrupted, which prevents the TDE from being a good precursor to the EMRI (Amaro-Seoane et al. 2017a).

However, the situation can be different for a massive star. Its tidal radius is much smaller than that of the main-sequence star, which will greatly shorten the time lag between TDE and EMRI. The lag time contour at as a function of initial semimajor axis a_0 and eccentricity e_0 is plotted in Figure 2. In the upper-left region, the lag time is shorter than 20 yr, which is ideal for observing the TDE and subsequent EMRI.

4. S/N of EMRI

The number of inspiral cycles in the frequency range $[f_{\rm min}, f_{\rm max}]$ is given by

$$N_{\rm cycles} = \int_{f_{\rm min}}^{f_{\rm max}} \frac{f}{\dot{f}} df. \quad (10)$$

Typically, the small body will spend 10^{4-5} cycles inspiraling into the SMBH, being observable for several years before plunge. The characteristic strain h_c of the GW from a source

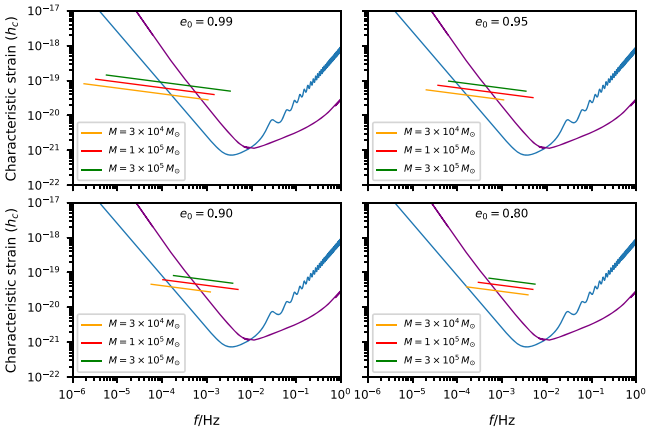

Figure 3. Diagram of an EMRI's characteristic strain h_c as a function of GW frequency f. For comparison, the sensitivity curves of LISA and Tianqin are plotted with blue and purple lines, respectively. Each panel is depicted with a certain initial orbit eccentricity e_0 and different BH masses. The mass of the C–O core is $3M_\odot$ and the redshift of the EMRI system is $z = 0.2$ for all panels.

emitting at frequency f is (Finn & Thorne 2000; Barack & Cutler 2004; Amaro-Seoane 2018; Maggiore 2018; Robson et al. 2019)

$$h_c(f) = 2f|\tilde{h}(f)| = \left(\frac{2f^2}{\dot{f}}\right)^{1/2} h_0 = \frac{(2\dot{E}/\dot{f})^{1/2}}{\pi D}, \tag{11}$$

where h_0 is the instantaneous root-mean-square amplitude, $\dot{E}$ is the GW emission power, and D is the proper distance to the source. In our model, the characteristic strain h_c is about 10^{-19}. It is worth mentioning that a fully coherent search of 10^{4-5} cycles for EMRI detection is computationally impossible. The feasible approach is hierarchical matched filtering by dividing data into short data segments (Gair et al. 2004, 2013). The S/N is built up in the second stage of the search by incoherently adding the power of short segments (Gair et al. 2004), which will decrease by a factor $N^{-1/4}$ than a fully coherent search, where N is the number of divided segments (Maggiore 2018). An incoherent search will be able to detect signals with S/N $\geqslant 20$; while in a fully coherent search, the S/N required for detection is $12 \sim 14$ (Amaro-Seoane et al. 2017a; Babak et al. 2017). The S/N can be estimated by (Maggiore 2018; Robson et al. 2019)

$$(\mathrm{S/N})^2 = \int_{f_1}^{f_2} \frac{h_c^2(f)}{h_n^2(f)} d(\ln f), \tag{12}$$

where $h_n^2(f) = fS_n(f)$ and $S_n(f)$ is the noise spectral density of the detector (Maggiore 2018). In our analysis, an S/N threshold of 36 is assumed for an incoherent search. Then EMRIs formed in our channel can be detected as far as $z \sim 1$ (about 3.4 Gpc). The foreground noise from WD binaries affects the detection of EMRIs, which has been discussed by many authors (Cornish & Larson 2003; Farmer & Phinney 2003). Some algorithms are used to subtract this noise (Cornish & Larson 2003) but their performances are rather uncertain. However, even assuming a 30% decrease of S/N after subtracting the WD background, the detection range will not be less than $z \sim 0.7$. The schematic diagram of an EMRI's characteristic strain h_c as a function of f is shown in Figure 3. LISA's sensitivity curve is generated from the online sensitivity curve generator—see Larson (2003).

The mass loss of the C–O core due to tidal stripping after entering the LISA band is less than 20%, which may not affect the detection of EMRIs.

5. Event Rate

In order to estimate the rate of EMRIs occurring in the universe, two ingredients must be considered. The first is the spatial density of SMBHs in the appropriate mass range. The second is the rate at which each black hole tidally disrupts massive stars. From observations, the space density of SMBHs can be approximated by $M_{\rm BH}$–σ relation

$$M_{\rm BH} = M_{\rm BH,*}\left(\frac{\sigma}{\sigma_*}\right)^{\lambda}, \tag{13}$$

where σ is the spheroid velocity dispersion. We use $\sigma_* = 90$ km s^{-1}, $\lambda = 4.72$, and $M_{\rm BH,*} = 3 \times 10^6\, M_\odot$ (Merritt & Ferrarese 2001). The above relation is derived from SMBHs with masses ranging from 10^6 to $10^9\, M_\odot$. For low-mass SMBHs ($<10^6 M_\odot$), Xiao et al. (2011) found that the $M_{\rm BH}$–σ relation is consistent with the above relation, allowing for the uncertainties. Therefore, the $M_{\rm BH}$–σ in Equation (13) is used in our derivation. The galaxy velocity dispersion function is constrained using galaxy luminosity functions and the L–σ correlation (Aller & Richstone 2002). Combined with the $M_{\rm BH}$–σ relation, the BH mass function is (Gair et al. 2004)

$$M_{\rm BH}\frac{dN}{dM_{\rm BH}} = \phi_* \frac{\epsilon}{\Gamma\left(\frac{\gamma}{\epsilon}\right)}\left(\frac{M_{\rm BH}}{M_{\rm BH,*}}\right)^{\gamma} \times \exp\left[-\left(\frac{M_{\rm BH}}{M_{\rm BH,*}}\right)^{\epsilon}\right], \tag{14}$$

where $\epsilon = 3.08/\lambda$, ϕ_* is the total number density of galaxies, and $\Gamma(z)$ is the gamma function. Aller & Richstone (2002) derived the parameters ϕ_*, $M_{\rm BH,*}$, and γ for different types of galaxies. For the mass range of interest in this analysis, $M_{\rm BH} < 10^6 M_\odot$, the parameters are $\phi_* = 36.7\, h_{70}^2$ Mpc^{-3}, $M_{\rm BH,*} = 4 \times 10^6 M_\odot$ and $\gamma = 0.03$. The spatial density of BHs is approximately

$$M_{\rm BH}\frac{dN}{dM_{\rm BH}} = 2 \times 10^{-3} h_{70}^2\ \mathrm{Mpc}^{-3}, \tag{15}$$

where $h_{70} \equiv H_0/70$ km s^{-1} Mpc^{-1} is the dimensionless Hubble parameter.

The rate at which each SMBH disrupts massive stars can be calculated using the loss cone theory (Magorrian & Tremaine 1999; Wang & Merritt 2004). For solar-type stars, the disruption rate per galaxy is (Wang & Merritt 2004)

$$\mathcal{R} = 6.5 \times 10^{-4}\ \mathrm{yr}^{-1}\left(\frac{M_*}{M_\odot}\right)^{-1/3} \times \left(\frac{R_*}{R_\odot}\right)^{1/4}\left(\frac{M_{\rm BH}}{10^6 M_\odot}\right)^{-1/4}. \tag{16}$$

Using the standard Salpeter initial mass function, the number ratio of 15–40$M_\odot$ stars to solar-type stars is 1.4×10^{-2}. The lifetime ratio of a massive star with $15M_\odot$ to a solar-type star is about 10^{-3}. In addition, the typical density of the He envelope is 10^3 times larger than that of solar-type star, so the tidal radius is one order of magnitude smaller. Hence, the rate should be

lowered by another factor of 10^{-3}. In addition, for our scenario to work, it is required that the star be on the He main sequence, whose duration lasts roughly 0.1 times that of the H main sequence. Combining all of the above factors and integrating Equation (15) over $15\,M_\odot < M_* < 40\,M_\odot$, $0.2R_\odot < R_* < 8R_\odot$, the event rate is $2 \times 10^{-4}\,\mathrm{Gpc^{-3}\,yr^{-1}}$ for $M_{\rm BH} = 5 \times 10^5 M_\odot$.

Below, we briefly discuss how to identify this type of EMRI. From the spectrum of the flare, the redshift of the tidal stripping event can be measured and the host galaxy can be localized. After a few tens of years, LISA may be able to detect EMRI signals in the same direction, which will determine the sky location to a few square degrees and the luminosity distance to 10% precision (Babak et al. 2017). Combining the redshift information from the flare with host galaxy properties, we can determine whether the flare and the EMRI occur in the same galaxy.

6. Summary

EMRI is a promising tool with which to study the strong field gravity, the stellar dynamics in galactic nuclei, massive BH populations (Babak et al. 2017; Amaro-Seoane 2018), and many other aspects of astrophysics. In this Letter, we propose a new formation channel for EMRIs, in which the tidal disruption flares can serve as EM precursors. The event rate of this type of EMRI is about $2 \times 10^{-4}\,\mathrm{Gpc^{-3}\,yr^{-1}}$. Combined with relevant EM signals, EMRIs will serve as a new standard siren to probe the expansion of universe.

We thank the anonymous referee for useful suggestions that were helpful in improving the manuscript. We thank W.-B. Han, X. Chen, and Ik Siong Heng for helpful discussions. This work is supported by the National Natural Science Foundation of China (grants U1831207, 11773010, U1738132, 1573014, and 11833003) and the National Key Research and Development Program of China (grant No. 2017YFA0402600).

ORCID iDs

Y. Y. Wang https://orcid.org/0000-0002-3822-0389
F. Y. Wang https://orcid.org/0000-0003-4157-7714
Y. C. Zou https://orcid.org/0000-0002-5400-3261
Z. G. Dai https://orcid.org/0000-0002-7835-8585

References

Abbott, B. P., (LIGO Scientific Collaboration and Virgo Collaboration), et al. 2017a, PhRvL, 119, 161101
Abbott, B. P., (LIGO Scientific Collaboration and Virgo Collaboration), et al. 2017b, Natur, 551, 85
Aller, M. C., & Richstone, D. 2002, AJ, 124, 3035
Amaro-Seoane, P. 2018, LRR, 21, 4
Amaro-Seoane, P., Gair, J. R., Freitag, M., et al. 2017a, CQGra, 24, R113
Amaro-Seoane, P., Audley, H., Babak, S., et al. 2017b, arXiv:1702.00786
Babak, S., Gair, J., Sesana, A., et al. 2017, PhRvD, 95, 103012
Barack, L., & Cutler, C. 2004, PhRvD, 69, 082005
Bloom, J. S., Giannios, D., Metzger, B. D., et al. 2011, Sci, 333, 203
Bogdanović, T., Cheng, R. M., & Amaro-Seoane, P. 2014, ApJ, 788, 99
Burrows, D. N., Kennea, J. A., Ghisellini, G., et al. 2011, Natur, 476, 421
Carter, B., & Luminet, J. P. 1982, Natur, 296, 211
Chen, H. Y., Fishbach, M., & Holz, D. E. 2018, Natur, 562, 545
Cornish, N. J., & Larson, S. L. 2003, PhRvD, 67, 103001
Cutler, C. 1998, PhRvD, 57, 7089
Cutler, C., Kennefick, D., & Poisson, E. 1994, PhRvD, 50, 3816
Dai, L. X., Escala, A., & Coppi, P. 2013, ApJL, 775, L9
Danzmann, K. 2000, AdSpR, 25, 1129
Davies, M. B., & King, A. 2005, ApJL, 624, L25
Di Stefano, R., Greiner, J., Murray, S., & Garcia, M. 2001, ApJL, 551, L37
Evans, C. R., & Kochanek, C. S. 1989, ApJL, 346, L13
Farmer, A. J., & Phinney, E. S. 2003, MNRAS, 346, 1197
Finn, L. S., & Thorne, K. S. 2000, PhRvD, 62, 124021
Gair, J. R., Kennefick, D. J., & Larson, S. L. 2006, ApJ, 639, 999
Gair, J. R., Barack, L., Creighton, T., et al. 2004, CQGra, 21, S1595
Gair, J. R., Vallisneri, M., Larson, S. L., & Baker, J. G. 2013, LRR, 16, 7
Gezari, S., Chornock, R., Rest, A., et al. 2012, Natur, 485, 217
Guillochon, J., & Ramirez-Ruiz, E. 2013, ApJ, 767, 25
Hannuksela, O. A., Wong, K. W. K., Brito, R., Berti, E., & Li, T. G. F. 2019, NatAs, 3, 447
Hayasaki, K., Stone, N., & Loeb, A. 2013, MNRAS, 434, 909
Hayasaki, K., Zhong, S. Y., Li, S., Berczik, P., & Spurzem, R. 2018, ApJ, 855, 129
Heger, A., Fryer, C. L., Woosley, S. E., Langer, N., & Hartmann, D. H. 2003, ApJ, 591, 288
Hills, J. G. 1975, Natur, 254, 295
Hjellming, M. S., & Webbink, R. F. 1987, ApJ, 318, 794
Hopman, C., & Alexander, T. 2005, ApJ, 629, 362
Hu, W. R., & Wu, Y. L. 2017, Natl. Sci. Rev., 4, 685
Kobayashi, S., Laguna, P., Phinney, E. S., & Mészáros, P. 2004, ApJ, 615, 855
Larson, S. L. 2003, Online sensitivity curve generator, http://www.srl.caltech.edu/shane/sensitivity/MakeCurve.html
Lodato, G., King, A. R., & Pringle, J. E. 2009, MNRAS, 392, 332
Lodato, G., & Rossi, E. M. 2011, MNRAS, 410, 359
Luo, J., Chen, L. S., Duan, H. Z., et al. 2016, CQGra, 33, 035010
MacLeod, M., Ramirez-Ruiz, E., Grady, S., & Guillochon, J. 2013, ApJ, 777, 133
Maggiore, M. 2018, Gravitational Waves, Vol. 2 Astrophysics and Cosmology (Oxford: Oxford Univ. Press), 2
Magorrian, J., & Tremaine, S. 1999, MNRAS, 309, 447
Merritt, D., Alexander, T., Mikkola, S., & Will, C. M. 2011, PhRvD, 84, 044024
Merritt, D., & Ferrarese, L. 2001, ApJ, 547, 140
Peters, P. C. 1964, PhRv, 136, 4B
Phinney, E. S. 1989, in IAU Symp. 136, The Center of the Galaxy, ed. M. Morris (Dordrecht: Kluwer), 543
Phinney, E. S. 2002, Presentation to the LISA International Science Team [LIST], 12 December 2001 (http://www.its.caltech.edu/~esp/lisa/LISTwg1.req-pr.pdf)
Pols, O. R. 2011, Stellar Structure and Evolution (Utrecht: Astronomical Institute)
Rees, M. J. 1988, Natur, 333, 523
Robson, T., Cornish, N. J., & Liu, C. 2019, CQGra, 36, 105011
Sigurdsson, S., & Rees, M. J. 1997, MNRAS, 284, 318
Strubbe, L. E., & Quataert, E. 2009, MNRAS, 400, 2070
Ulmer, A. 1999, ApJ, 514, 180
Wang, J., & Merritt, D. 2004, ApJ, 600, 149
Wang, Y. Y., & Wang, F. Y. 2019, ApJ, 873, 39
Wang, Y. Y., Wang, F. Y., & Zou, Y. C. 2018, PhRvD, 98, 063503
Woosley, S. E., Heger, A., & Weaver, T. A. 2002, RvMP, 74, 1015
Xiao, T., Barth, A. J., Greene, J. E., et al. 2011, ApJ, 739, 28
Yuan, W. M., Zhang, C., Feng, H., et al. 2015, arXiv:1506.07735
Zauderer, B. A., Berger, E., Soderberg, A. M., et al. 2011, Natur, 476, 425